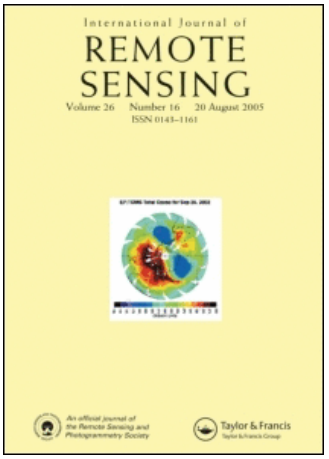

International Journal of Remote Sensing
Publication details, including instructions for authors and subscription information:
http://www.informaworld.com/smpp/title~content=t713722504

Single and two epoch analysis of ICESat full waveform data over forested areas

V. H. Duong [a]; R. Lindenbergh [a]; N. Pfeifer [b]; G. Vosselman [c]
[a] Delft University of Technology, Delft Institute of Earth Observation and Space systems, the Netherlands
[b] Vienna University of Technology, Institute of Photogrammetry and Remote Sensing, Austria
[c] International Institute for Geo-Information Science and Earth Observation - ITC, the Netherlands

Online Publication Date: 01 March 2008
To cite this Article: Duong, V. H., Lindenbergh, R., Pfeifer, N. and Vosselman, G. (2008) 'Single and two epoch analysis of ICESat full waveform data over forested areas', International Journal of Remote Sensing, 29:5, 1453 - 1473
To link to this article: DOI: 10.1080/01431160701736372
URL: http://dx.doi.org/10.1080/01431160701736372

International Journal of Remote Sensing
Vol. 29, No. 5, 10 March 2008, 1453–1473

Taylor & Francis
Taylor & Francis Group

Single and two epoch analysis of ICESat full waveform data over forested areas

V. H. DUONG*†, R. LINDENBERGH†, N. PFEIFER‡ and G. VOSSELMAN§
†Delft University of Technology, Delft Institute of Earth Observation and Space systems, the Netherlands
‡Vienna University of Technology, Institute of Photogrammetry and Remote Sensing, Austria
§International Institute for Geo-Information Science and Earth Observation – ITC, the Netherlands

Analysis of full-waveform pulses from space-based laser altimeter systems are expected to improve our ability of measuring forests globally. Moreover, with the increase in the number of waveform data sets, it is now possible to study temporal changes in waveform returns over the same spatial domain. ICESat full waveform data from two epochs, i.e. winter and summer (2003) along near-coincident ground tracks, are studied. Data analysis methods are discussed, including normalization and matching of near-coincident waveforms, Gaussian decomposition, and derivation of forest measurement and forest change parameters. We quantify differences between winter and summer waveforms, acquired over broad-leaved, mixed-wood, and needle-leaved forests in Europe. The results indicate that, although maximum tree height barely changes over six months, i.e. $<2.2\%$ for all three cover types, the Height of Median Energy (HOME) changed most in broad-leaved (a 148% change) and least for conifers (a 36% change, winter to summer). Ratios of ground energy to canopy energy of normalized waveforms also changed noticeably over time: 67% in broad-leaved, 62% in mixed-wood, and 47% in conifers. Attempts are made to differentiate and classify these three cover types on the basis of these and other canopy metrics. The initial results, with a coefficient κ of agreement between reference and classified data of 0.57, provide a baseline against which improvements in data and methodology can be gauged.

1. Introduction

Characterization and quantification of forest canopy structure across extensive areas challenge remote sensing scientists (Harding 2001). Forest canopy structure is defined as 'the organization in space and time, including the position, extent, quantity, and connectivity, of the aboveground components of vegetation' (Parker 1995), and plays a key role in developing a better understanding of how forest ecosystems function (Drake *et al.* 2002). The forest canopy is also defined as 'the collection of all leaves, twigs, and branches formed from the combination of all the crowns in the stand' (Maser 1989), and is responsible for the majority of material and energy exchanges with the atmosphere (Lefsky *et al.* 1999). However, accurate estimation of aboveground forest biomass at regional/subcontinental scales remains

*Corresponding author. Email: v.h.duong@tudelft.nl

International Journal of Remote Sensing
ISSN 0143-1161 print/ISSN 1366-5901 online
http://www.tandf.co.uk/journals
DOI: 10.1080/01431160701736372

a major obstacle when using conventional remote sensing techniques (Dubayah *et al.* 1997).

Currently a new generation of advanced laser altimetry systems overcomes several limitations of conventional approaches for estimating forest structure, like aboveground biomass and tree height. These advanced systems record a full vertical profile of data in the forest within small-sized footprints (a few centimetres with RIEGL LMS-Q560, OPTECH ALTM 3100, and TopEye MKII), medium-sized footprints (approximately 10–25 m with SLICER and LVIS) and large-sized footprints (ICESat, 70 m). SLICER stands for Scanning Lidar Imager of Canopies by Echo Recovery. LVIS is the Lidar Vegetation Imaging Sensor that superseded SLICER. Both SLICER and LVIS are airborne Lidar systems but SLICER no longer exists because parts of it were used to build LVIS (Harding 2000).

ICESat abbreviates Ice, Cloud and land Elevation Satellite. The ICESat spaceborne laser altimeter system was launched in January 2003 with the principal objectives to measure polar ice-sheet elevation change, atmospheric profiles of cloud and aerosol properties, land topography profiles referenced to a global datum, and height of vegetation canopies (Zwally *et al.* 2002). These objectives are accomplished through the use of the Geoscience Laser Altimeter System (GLAS), in combination with precise orbit determination. GLAS uses a laser altimeter to measure the range between the satellite and the earth surface. The instrument time stamps each laser pulse emission, and measures the echo pulse waveform from the surface. GLAS acquires elevation profiles of the entire earth along tracks that are revisited in a 183-day repeat cycle, with 70 m diameter footprints spaced every 175 m. A waveform, recording laser back-scatter energy as a function of time, is digitized in 544 consecutive bins at a temporal resolution of 1ns over land for each footprint (NSIDC 2005a). The land waveform of 15 cm vertical resolution yields an 81.6 m height range (544 waveform bins $\times$ 15 cm per bin) for laser L1 and 150 m (1000 bins $\times$ 15 cm per bin) for laser L3 (Harding 2005). GLAS carries three different laser altimeters, L1, L2 and L3. Laser 1 was turned off shortly after the Spring 2003 campaign, to be replaced by Laser 2. Laser L2 operates in both height ranges.

The method of full waveform analysis has been investigated by many scientists for classification and calculation of forest structure parameters. It was applied to specify forest species of different kinds (Ranson *et al.* 2004, Reitberger *et al.* 2006), to identify land cover types (Duong *et al.* 2006), and to separate vegetation from non-vegetation classes (Ducic *et al.* 2006). In addition, estimation of forest parameters from full waveform processing has been studied. Forest parameters, like maximum canopy height and aboveground biomass, were extracted from the full waveform data and compared to field measurements taken from the same location. A strong correlation between laser full waveform measured canopy height and aboveground biomass has been found by Harding (2001), Drake *et al.* (2002) and Lefsky *et al.* (2002). Finally, forest height was estimated from ICESat waveforms, in combination with a measure of topographic relief (Lefsky *et al.* 2005). In this paper, a new method for analysing individual waveforms and pairs of waveforms for the derivation of forest structure parameters is introduced.

The purpose of this paper is twofold. First, it seeks to extract forest parameters from single shots of a satellite-borne full waveform laser altimeter. Second, it attempts to show the utility and limitations of analysing ICESat waveform pairs acquired over roughly the same footprint during leaf-off and leaf-on seasons. The

first objective means a change of paradigm in extracting forest parameters from laser scanning data. So far, high point densities (typically 1–10 points m^{-2}) of discrete return laser altimetry data have been used (Næsset *et al.* 2005). Data are typically acquired in dedicated missions and information is provided at the stand level. The latter is necessary because a sufficient amount of information (discrete backscattering points) is required for deciding which points are above the ground and which are on the actual ground, and for linking forest parameters to point observations via statistical procedures. We aim to demonstrate the derivation of forest parameters on the basis of the footprint area of individual, full waveform laser-ranging measurements. Limitations imposed by GLAS data characteristics, e.g. spatial misregistration, changes in footprint size and laser power, can only be partially mitigated, making conclusions concerning forest structural change over time difficult, but not impossible.

The second objective, i.e. using repeatedly-measured ground spots for deriving forest change metrics, is an extension of the shot-based approach in a multi-temporal embedding. To achieve this objective, ICESat full waveform data from two different epochs are compared and combined. One data set was acquired by Laser 1, L1, in winter, February 2003, the other by Laser 2, L2, in summer, September 2003. The two data sets are obtained from repeated tracks and therefore many pairs of footprints from both data sets exist that overlap entirely in the ideal case and at least have some common topographic intersection in all other cases. Because we use different lasers, the intensities of corresponding waveforms from winter and summer are not comparable and we consequently consider normalized waveforms. Also atmospheric attenuation is not necessary the same. Using a full waveform analysis, forest parameters of both data epochs are calculated and compared: maximum canopy height (*MCH*), height of median energy (*HOME*), ratio between total intensity of ground return and canopy return (*GRDRT*), and canopy intensity difference (ΔI). This paper proposes a direct way of determining the change in forest structure by seasonal influences from pairs of waveforms within at least partly overlapping footprints. As an application, but mainly as a method of validation, general forest waveform pairs are classified into forest types, resulting in a kappa value of $\kappa=0.57$.

In §2 we first describe several processing steps that precede the actual inter-epoch waveform comparison. We explain how the waveforms can be standardized via normalization and shift operations, but also how to fit Gaussian components to the waveforms. Subsequently, a method of comparing normalized waveforms is introduced. In §3, we present our data set and give the results of the comparison between summer and winter waveforms. Problems with the current data set, mainly caused by shot-to-shot misregistration and by the effects of topography on the waveform, are identified and discussed. Although the data used here are from ICESat, the methods that are described can also be generalized and applied to other waveform LiDAR data sets.

2. Methodology

ICESat's data distribution consists of 15 data products called GLA01, GLA02, …, GLA15 (Brenner *et al.* 2003). In this study, we investigated the product GLA01, the global full waveform data, and GLA14, the global land surface altimetry data. The latter product was obtained after precise geolocation and was used for the

visualization of the ICESat groundtracks (figure 1) as well as for local slope determination (§3.7).

2.1 *Waveform normalization*

The voltage waveform was first normalized to enable a comparison of waveforms captured in different epochs. For example, due to different atmospheric conditions or changes in the behaviour of the laser device, the amount of energy in the laser return pulse may vary with time, even if the ground has not changed at all. These effects aggravated a comparison of absolute energy levels of particular constituents of different waveforms. The normalization step required a division of the received energy V_i by the total energy V_T, at moment i (see equation 1). After normalization the area under any waveform equaled 1 (see figure 2):

$$V_N(i) = \frac{V_i}{V_T}, \qquad \text{with} \qquad V_T = \sum_{i=1}^{N} V_i \tag{1}$$

where N is the number of waveform bins. In this study N equaled 544.

2.2 *Real signal of waveforms*

Raw waveforms contain ambient system noise at the beginning and end of the waveform signal (figure 2). Therefore, the real signal of the waveform was found by thresholding the raw waveform. The threshold value for each raw waveform was individually identified by calculating the mean and standard deviation of the noise at the first 100 ns range of the raw waveform. As such the threshold value was determined as the mean plus four times the standard deviation (Lefsky *et al.* 2005). The signal value at that part of the waveform that was below the threshold was set to zero (see figure 3).

2.3 *Smoothing the waveform for initial parameter estimation*

Decomposition of waveforms with Gaussians was proposed by Brenner *et al.* (2003). The methods for smoothing and the derivation of the number of modes as well as their approximate values were developed within our group at Delft University of Technology. From the real waveform signal initial parameters needed to be identified for the fitting step, e.g. number of peaks or modes together with width, amplitude and location for each mode. Due to the rough shape of many waveforms, estimation of initial values resulted in a large number of modes with a low amplitude and a narrow width. Therefore, it was necessary to smooth the waveforms in order to get a smaller number of modes (Brenner *et al.* 2003).

The normalized waveforms were therefore smoothed, using a Gaussian filter. In this filter approach, weights for available observations were obtained by the relative height of a Gaussian shape at an observation location. The Gaussian shape was positioned such that its maximum coincided with the filtering location. Furthermore, the width of the Gaussian shape was defined via the standard deviation (sigma). However, when the Gaussian is used for smoothing, it is common to describe the width of the Gaussian by the Full Width at Half Maximum ($FWHM$). The $FWHM$ was related to sigma by the formula: $FWHM = 2.35 \times \sigma$. We

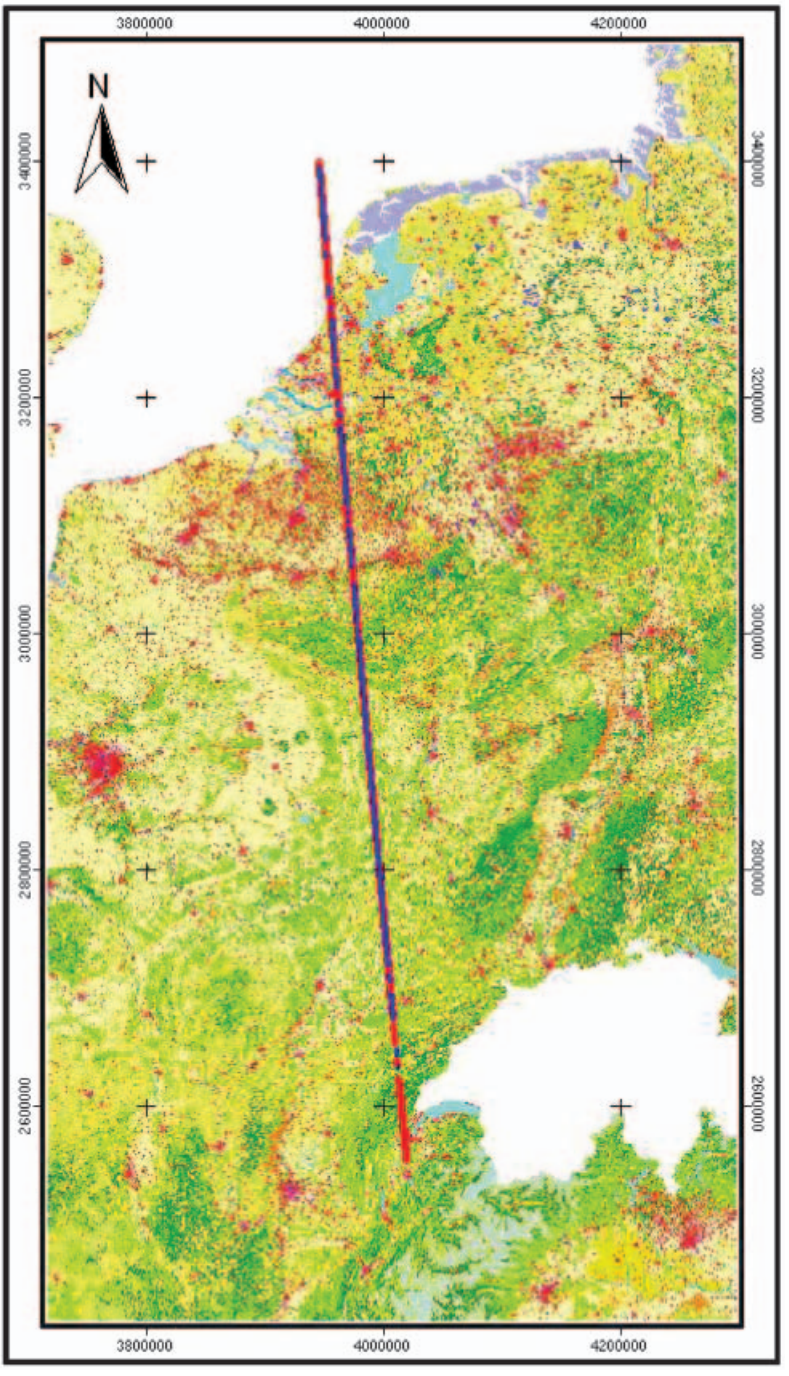

Figure 1. ICESat groundtracks from February (blue) and September 2003 (red) overlaid on the CORINE land cover image.

used a *FWHM* value of 45 cm (three times vertical resolution) for the smoothing step. Following this step, we could estimate the locations and amplitudes of the peaks in the smoothed waveform.

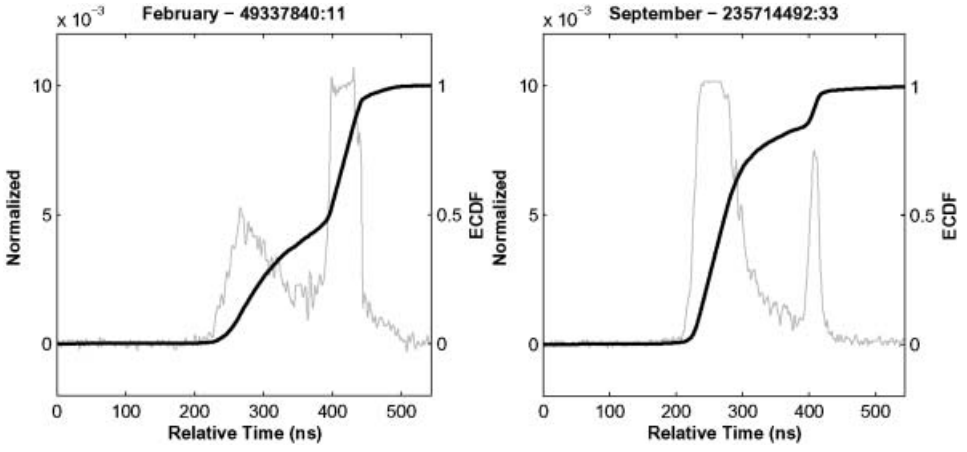

Figure 2. Two normalized waveforms that are approximately at the same spot from February, 2003 (on the left, grey) and from September, 2003 (on the right, grey), are displayed together with their cumulative distribution curve (in black).

To avoid small and noisy peaks, a search window of 75 cm wide (five neighbouring height bins) was selected to estimate peak locations. The window moved from the beginning to the end of the waveform with an interval of one vertical 15 cm height bin. If the waveform value at the middle of the window was higher than at the four other window positions, and if, in addition, the direct neighbours on the left and the right were higher than the two boundary points, then the centre position was considered as the location of a peak. The amplitude of the peak was extracted from the waveform at the peak location. Finally, an initial

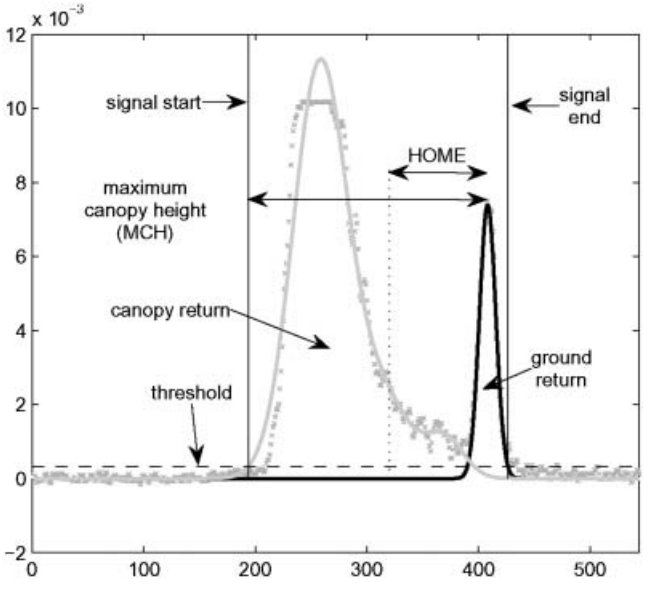

Figure 3. Waveform parameters: maximum canopy height (MCH=32.15 m (214.3 ns)), canopy return, ground return, height of median energy ($HOME$=20.60 m (137.3 ns)). The $GRDRT$ for this waveform is 0.16.

approximate mode width was calculated as half the distance between two neighbouring peaks. The distance between neighbouring peaks was set to be at least 1.5 m.

2.4 *Fitting algorithm*

In the fitting step, Gaussian components were fitted to the normalized waveform $w(t)$. Every Gaussian component W_m corresponded to one Gaussian bell curve and the waveform $w(t)$ was decomposed into a series of Gaussian components W_m. We thus write

$$w(t) = \sum_{m=1}^{N_p} W_m(t), \qquad \text{with} \qquad W_m = A_m e^{\frac{-(t-t_m)^2}{2\sigma_m^2}} \tag{2}$$

where $w(t)$ is the waveform at time t, $W_m(t)$ is the contribution of the m^{th} Gaussian component, N_p is the number of Gaussians found in the waveform, A_m is the amplitude of the m^{th} Gaussian, t_m its position and σ_m its standard deviation.

The least-squares method was used to compute the model parameters. That is, the values for A_m, t_m, and σ_m in equation (2) were obtained by fitting the theoretical model to the observed waveform in such a way that the difference between model and observation was minimized in the least squares sense. Alternative, (partly) similar fitting algorithms were described by Carabajal *et al.* (1999), Hofton *et al.* (2000), Brenner *et al.* (2003), Wagner *et al.* (2006), Persson *et al.* (2005), Jutzi *et al.* (2005) and Reitberger *et al.* (2006). The fitting method was implemented using the conditions described below.

(i) The number of Gaussian components was limited to six.
(ii) The minimum distance between neighbouring peaks was 1.5 m.
(iii) The minimum amplitude of an individual peak equaled the noise threshold value as described above.
(iv) The minimum sigma of an individual peak was 30 cm.

A maximum iterations of 10 was used in the fitting procedure, which was stopped when the result met the criteria above. When the conditions were not met, the waveform could not be fitted and was discarded. Moreover, the square sum of the residuals was used to quantify the quality of the fit. Two results of the fitting algorithm are shown in figure 4. Four modes were found in the summer waveform (right) and five modes in the winter waveform (left).

In the following, we will refer to the right-most Gaussian component of the waveform decomposition as the last mode, as this mode corresponds to the energy reflected by the surface hit last (see figure 4). In forest applications, the last mode will generally correspond to the bare earth below the trees, as long as the earth surface is not completely occluded by vegetation. The left-most Gaussian component will be referred to as the first mode, as this component corresponds to the first feature in the laser footprint that reflects the laser light. Over forest areas, the first mode mostly originated from reflections by the tree canopy.

2.5 *Shift computation*

The raw waveform was distributed as the GLA01 product, but the GLA01 data were not georeferenced. GLA14 data were georeferenced, and the link between the two data sets was a common, unique index number associated with each shot. Each

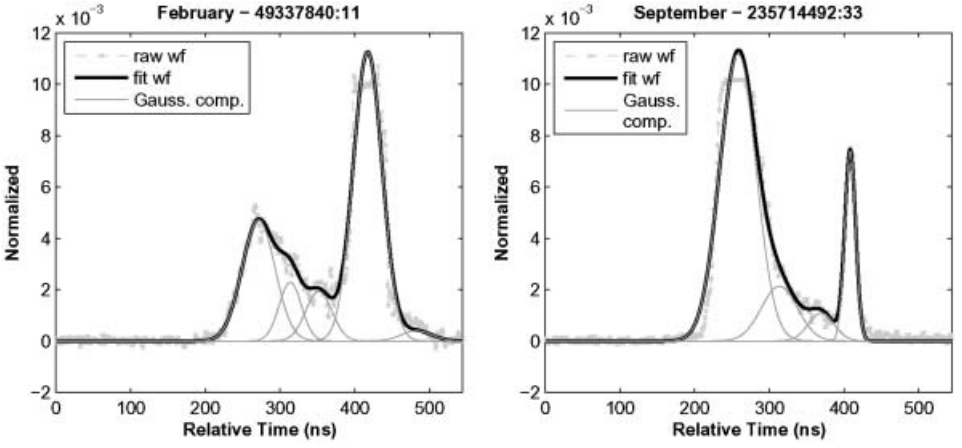

Figure 4. Two fitted waveforms (black solid) are displayed together with the raw waveform (grey starred line) and the Gaussian components (grey solid) for February, 2003 (left) and September, 2003 (right).

winter and summer GLA01 waveform was annotated with the corresponding GLA14 shot location. Coincident or near-coincident winter and summer GLAS shots were identified based on their geographic coordinates. Once multitemporal (winter/summer) pairs were identified, the paired, normalized waveforms had to be aligned. Optimal shift parameters were computed in order to make the normalized waveforms comparable along the waveform amplitude axis (y-axis).

The shift computation can be performed on the complete waveform (Hofton *et al.* 2002) or on just its last mode. The complete waveform gave good matching results in case of similar waveform shapes in two epochs. The last mode method was useful in case of rather different waveform shapes in the two epochs. In the latter case, the ground surface was assumed to be stable, which implied that the last modes of the two epochs should be matching. However, the waveform sometimes had a 'tail' on the side of the last mode, which was a small Gaussian mode found by the fitting algorithm (see figure 4, on the left). Such a tail mode was not considered to be the correct ground truth. A modified last mode method was therefore developed, which was expected to result in a better match. If the amplitude ratio of the last mode and the second-to-last mode was less than 15 percent, the last mode was removed and the second-to-last was implemented as the new last mode. The new decomposition result was determined by removing the small last mode from the previous decomposition result without any need of repeating the decomposition step.

For a given pair of coincident, winter/summer, normalized waveforms, the shift is found by determining that time shift m, for $m=1, \ldots, 2N-1$, that minimizes the length of the cross-correlation sequence $\left\|\widehat{R}_{xy}(m)\right\|$ between the normalized waveforms of February, W_F and September, W_S. The cross-correlation $\widehat{R}_{xy}(m)$, (Press *et al.* 1992), for time shift m is defined as

$$\widehat{R}_{xy}(m) = \begin{cases} \sum_{n=0}^{N-m-1} x_{n+m} y_n^* & m \geq 0 \\ \widehat{R}_{xy}^*(-m) & m < 0 \end{cases} \tag{3}$$

where x_n and y_n represent the discrete Fourier transforms of the normalized waveforms W_F and W_S. Note that in our case, N can be the length of the

entire waveform ($N=544$) or just the length of the last mode of the waveform ($N\approx100$).

The shift operation is illustrated in figure 5. The two last modes (peaks) of the summer and winter waveforms, recorded at approximately the same location in the same year, did not match. Therefore, a shift was determined with the cross-correlation method. This method gave an incorrect match (dash) based on the complete waveform due to the strong change in waveform shape. The shifted, dotted grey waveform based on the last mode was not a good match either, due to noise in the tail of the winter waveform. Employing the modified last mode approach, the noisy tail of the winter waveform was removed, producing a good match between the winter and summer waveforms.

2.6 *Waveform parameters for forest structure*

After the normalization and shift operation, we were able to quantify the difference in canopy between a corresponding summer and winter waveform by analysing the change in a number of parameters that described the canopy structure.

Consider two waveforms, one waveform W_F, from February and its corresponding waveform W_S, from September, both normalized and, in addition, matched by the shift operation. A forest waveform normally has two dominant peaks that represent the canopy portion (the left side of the waveform) and the ground portion. The true (modified) last mode of the fitting result was used as ground return and the remaining waveform, the difference between the full waveform (fitted) and the ground return, was used as the so-called canopy return.

Three parameters that describe forest structure were used in this investigation (see figure 3). First, a maximum canopy height (*MCH*), or tree height (Harding 2001), was defined as the distance from the position of the signal start of the waveform to the peak position of the ground return. Second, a height of median energy (*HOME*)

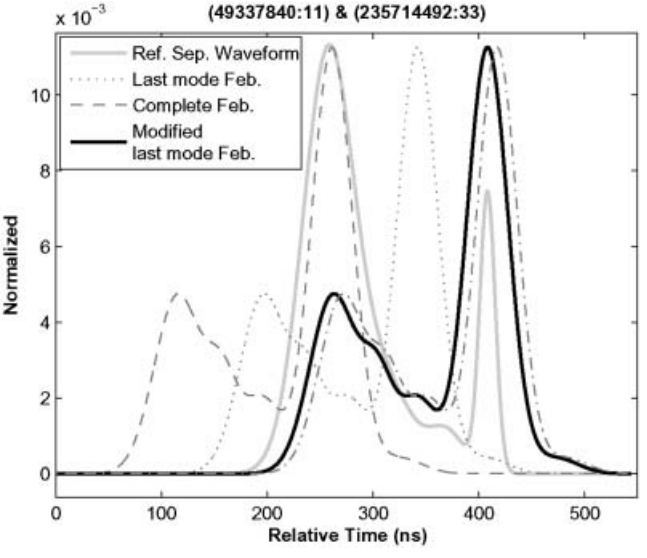

Figure 5. The original summer waveform is kept fixed (solid black, thick). An original winter waveform (solid black, thin) is shifted by last mode (dotted grey), by complete waveform (dash grey), and by modified last mode (grey solid).

(Drake *et al.* 2002) was defined as the distance from the peak of the ground return to the position of median energy of the fitted full waveform. Third, the ground return ratio (*GRDRT*) was calculated as the total energy of the ground return (the last mode), divided by the total energy of the canopy return.

The *MCH* or the tree height was not expected to change much between the winter and summer seasons. Therefore, differences in *MCH* between two epochs (ΔMCH) should be small. In analysing the results, the ΔMCH was used as validation. However, the *HOME*, a measure for the distribution of the returned energy, was found to be quite sensitive to changes in the canopy. For example, figure 4 shows a winter waveform (left) and a summer waveform (right) over a broad-leaved forest. The winter waveform clearly has a much smaller canopy return. This is reflected in the position of the median energy that is much closer to the ground. Finally, the ground/canopy ratio value (*GRDRT*) is sensitive to both the intensity return from the canopy and the ground. For the summer waveform, the intensity return is larger from the canopy and smaller from the ground. As a consequence, the *GRDRT* in figure 4 is small for summer and large for winter.

The canopy portion or canopy return of the waveform was defined as the difference between the fitted waveform and the last mode. Therefore the canopy intensity difference of a given pair of February/September waveforms was determined as the mean squared intensity difference of a pair of February/September canopy returns.

If VC_F and VC_S denote the intensities of the canopy return of the waveform in February and September, the canopy intensity difference was defined as follows:

$$\Delta I(WC_F, WC_S) = \sum_{i=1}^{K} \frac{(VC_F(i) - VC_S(i))^2}{K} \tag{4}$$

where K is the number of non-noise height bins in the canopy, i.e. non-ground portion of the normalized waveforms, WC_F and WC_S are the waveform canopy returns of February and September, and ΔI is the average of squared differences in normalized amplitudes.

For the comparison of W_F and W_S we introduced four parameters: a difference in maximum canopy height (ΔMCH); a difference in height of median energy ($\Delta HOME$); a difference in the ratio of total intensity between ground and canopy return ($\Delta GRDRT$); and the canopy intensity difference (ΔI). The differences between the four parameters were calculated under leaf-on and leaf-off conditions.

3. Results and discussion

3.1 *Test forest data*

3.1.1 ICESAT/GLAS full waveform data. ICESat data were downloaded from the National Snow and Ice Data Center (NSIDC 2005b). The data we analysed belong to a track covering part of the Netherlands, Belgium and France. The GLA14 was used to visualize the geolocation of the waveform data, which appears as a straight line in figure 1. The ICESat data used in this area stemmed from two epochs, one from 27-02-2003 (winter season, blue track) and the other from 30-09-2003 (end of summer season, red track). The ICESat footprint had elliptical shapes with an average size of 95 m × 52 m (Abshire 2005) for the winter data. The azimuth of the major axis was 162.5°. The summer data had an average footprint size of 87 m × 43 m, with an azimuth of 184.2°. The attributes of the footprints, major and

minor axes, and the azimuth angle of the major axis that described the summer data were provided as metadata from the NSIDC. However, the footprint attributes for the winter acquisition were taken from Abshire (2005) because of operational errors associated with the winter data acquisition.

There were 2848 waveforms in the winter season data set and 4358 waveforms in the summer one (see table 1). The waveform data of both epochs were decomposed into Gaussian components. The number of fitted waveforms was 2775 (97% fitted successfully) in winter, and 4284 (98%) in summer. These numbers were comparable to the fitting success figure of 98% reported by Wagner *et al.* (2006) for small footprint airborne full waveform laser scanning from a flying height of 500 m. The fitting and decomposition step sometimes did not give a solution for noisy waveforms that did not satisfy the condition outlined in §2.4. Moreover, the number of intersecting waveform footprints between epochs was 2600 before and 2363 after the decomposition step. The 2363 waveforms were then categorized in land cover types.

3.1.2 CLC2000 land cover data. The CORINE Land Cover 2000 database (CLC2000) was initiated by the European Environment Agency (EEA) and the Joint Research Centre (JRC). The CLC2000 database originated from the year 2000 but data were actually obtained during a three-year period from 1999 to 2001, with a horizontal geolocation accuracy of 25 m based on satellite images of Landsat 7 ETM+ with 25 m pixel resolution. The CLC2000 data product was obtained from the Landsat data via a computer-assisted visual interpretation of the satellite images, under the requirements of a scale of 1 : 100 000, a minimum mapping unit of 25 hectares and a pixel resolution of 100 m (Perdigao 1997). The CLC2000 classification was hierarchical and distinguishes 44 classes at the third level, 15 classes at the second level and five classes at the first level. Detailed information of land cover levels can be found at the metadata section of the CLC2000 on the European Environment Agency website (CLC2000 2006). The total thematic accuracy of the CLC2000 database was almost 95%. The database was georeferenced in the European reference system (Hazeu 2003).

The CLC2000 was reclassified into six land cover types: urban, bare land/low vegetation, water, broad-leaved forest, mixed forest, and needle-leaved forest. Pairs of decomposed waveforms were identified as belonging to one of these six land-cover types. The 2363 waveform pairs were divided into broad-leaved (deciduous, 440), needle-leaved (coniferous, 89), mixed (62), urban (170), bare land/low vegetation (1248) and water/sea (354). Before classifying waveforms, however, an additional step was needed to convert ICESat geolocation data (GLA14) to the

Table 1. Number of waveforms used.

Data	*Total*	*Fitted*	*Broad*	*Mixed*	*Needle*	*Urban*	*Bare*	*Water*
Feb-03	2848	2775	559	102	111	204	1444	355
Sep-03	4358	4284	702	130	201	455	2091	705
Overlap	2600	2363	440	62	89	170	1248	354
Number of modes (Feb/Sep)	N/A	2.1/2.0	3.3/3.5	3.9/3.5	3.2/3.3	2.3/2.2	1.8/1.5	1/1
Total Energy (Feb/Sep) $\times 10^{-15}$ J	3.7/8.6	3.7/8.4	4.9/9.0	7.2/10.1	6.6/6.7	3.5/10.9	3.3/9.8	2.1/1.6
WF extent (Feb/Sep) $\times$ m	N/A	14.3/13.2	23.0/28.1	30.3/28.4	26.7/24.8	13.4/12.8	11.9/9.3	6.7/2.6

coordinate system of CLC2000. The ICESat geolocation used the same ellipsoid as TOPEX/Poseidon and Jason-1 (radius of equator 6378 136.30 m and reciprocal flattening (1/f) 298.257 (NSIDC 2005a)). Therefore, the GLA14 geolocation data of two epochs were converted to WGS84 by a tool developed by the NSIDC and were then transformed into the European coordinate system (CLC2000 2006) by ArcGIS 9.0 software (www.esri.com). Finally, the ICESat geolocation were overlaid with the CLC2000 to classify the waveforms according to the land cover types.

3.2 *Footprint shifts*

On average, the distance between the centre points of corresponding footprints was 67.83 m. This may cause an inaccuracy in the change detection of forest areas. However, for flat or low relief area covered by homogeneous forest, we assumed that similar waveforms were returned from all over the area. In case of significant topographic relief or nonhomogeneous forests, a comparison of a single waveform pair was not expected to give accurate results, but considering many waveform pairs simultaneously was likely to result in interpretable average waveform changes. We could therefore detect seasonal changes in the forest structure by looking at averaged changes across near-coincident, paired footprints. In figure 6, the grey ellipse footprints represent data tracked in September 2003, while the black footprints were collected in February 2003.

3.3 *Intensity comparison*

The intensity, or the full returned energy of the waveform data, in September, tended to be larger than in February. This is illustrated in figure 7, where histograms of the intensities in February and in September are provided. The mean intensity differed by a factor of almost 2 (see table 1). One of the reasons for this difference was the change from GLAS laser L1 to laser L2 aboard of the ICESat satellite. Another reason was maybe caused by the foliage and herbaceous vegetation that

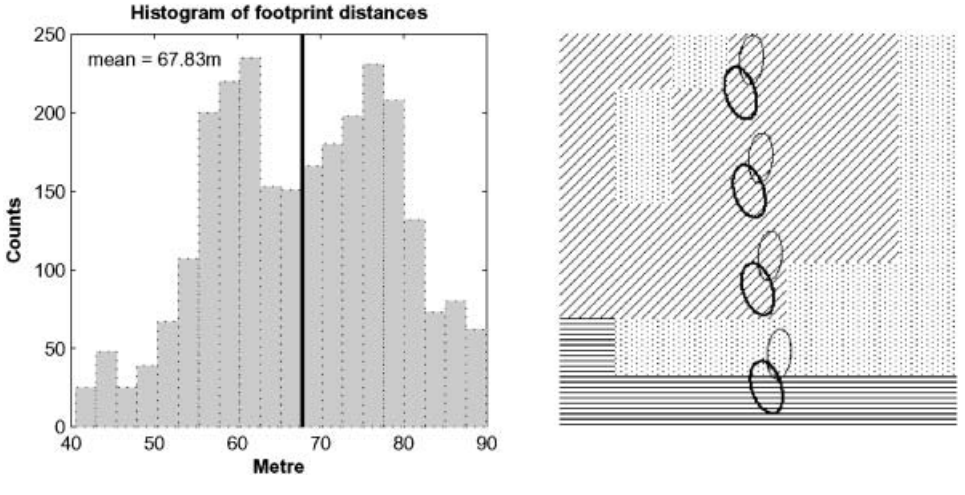

Figure 6. Histogram of footprint distances (left) and its mean (on left, vertical black line). Visualization of footprint locations (right) of winter (thick black) and summer (thin black) and the 100 m CLC2000 map with bare land (dot pattern), needle-leaved (horizontal line pattern) and broad-leaved (slant line pattern).

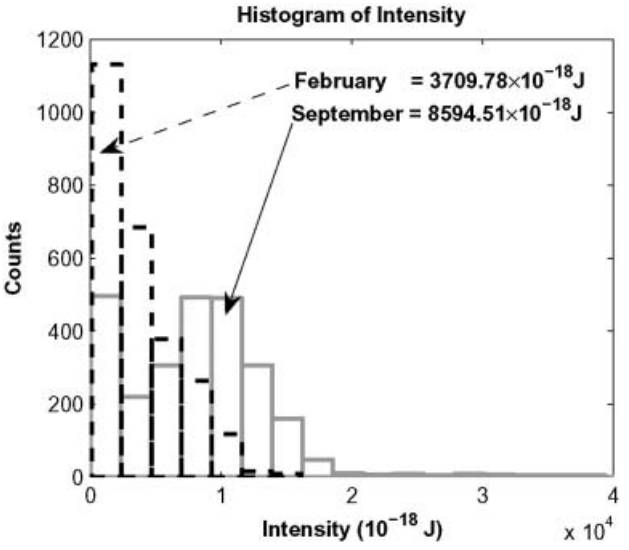

Figure 7. Two intensity histograms displayed together: February, 2003 (dashed) and September, 2003 (grey) with its mean intensity. The mean intensity of the summer data is 2 times the mean intensity of the winter data.

was more prevalent in September, permitting less absorption of the emitted laser energy in the near infrared laser wavelength. This could explain the large differences in average intensity return; for example, the broad-leaved and the bare land classes. As a consequence, we could not directly compare waveforms from the two different seasons (confirmed by NSIDC). Therefore, relative intensities, which were obtained by the waveform normalization step, will be considered in subsequent steps.

3.4 *Waveform shifts*

As mentioned in Section 2.5, observed shifts occurred between pairs of non-georeferenced GLA01 waveforms. As these shifts did not reveal a clear pattern, a local shift was determined for each pair of summer–winter waveforms.

The results reported in table 2 indicated that the 3 shift calculation approaches generated similar shifts: approximately −2.7 m, for water, bare land/low vegetation, and urban areas. The matching result was different for broad-leaved, needle-leaved and mixed forest in the three methods. For broad-leaved, the difference between the complete waveform matching and the two last mode methods was quite large, i.e. in the order of 7 m. The matching results for mixed forest were similar to the broad-leaved case. Finally, for needle-leaved forest, the matching result was quite similar for the three methods compared to the matching results of the broad-leaved and mixed, but the difference between the complete waveform method and the two

Table 2. Shifting comparison (metre).

Based on	*Broad*	*Mixed*	*Needle*	*Urban*	*Bare*	*Water*
Last mode	−0.45	−6.15	−8.55	−2.70	−2.85	−2.25
Modified last mode	−0.60	−6.45	−9.00	−3.00	−3.00	−2.25
Complete waveform	6.60	−4.20	−7.20	−3.30	−3.45	−2.25

others was still large (≈1.5 m) compared to the difference of the other two methods (≈0.5 m).

The shift calculated for forest waveform pairs was generally larger than for waveforms in open terrain. This might be caused by the following reasons:

- The returned waveforms or waveform pairs from the forest areas had more complicated shapes and a greater noise component relative to waveforms in open areas.
- The waveform pairs were not spatially co-registered, and this misregistration error is exacerbated in high relief areas. In some cases, paired waveforms did not measure the same forest cover types.
- Waveforms returned from high relief terrain or from terrain covered by dense forest had wide last modes.
- In some cases, the last mode was not identified properly by the fitting algorithm.
- The waveforms from areas of dense forest may only have represented forest canopy, in case no laser light could penetrate to the ground.
- The larger normalized waveform shifts between paired broad-leaved shots could be explained by the sensitivity of the centroid of a waveform to seasonal foliage changes.

In this paper, we assumed that the ground return is stable. As a consequence, the use of the last mode of the decomposition result was considered more reliable in the matching step. Because the complete waveform method occasionally resulted in a wrong match, and because a large second-to-last mode was sometimes trailed by a small last mode, the matching result from the modified last mode method was employed in subsequent analyses.

One should be careful in drawing physical conclusions based on the shift results presented here, as these shifts are not exactly co-registered with respect to the latitude/longitude and illuminated area. In order to determine if the last mode, assumed to represent the surface height, matches between summer and winter waveforms, the raw GLA01 waveforms should be combined with the GLA14 altimetry data in order to obtain 'georeferenced waveforms'. The height given in the GLA14 product refers to the centroid of a waveform, Harding (2005). By overlaying georeferenced summer/winter waveforms, a potential shift in the last mode can be identified. The larger (non-georeferenced) shifts observed for broad-leaved forests can be explained by the sensitivity of the centroid of a waveform to seasonal foliage changes.

Shifts of the last mode between overlapping waveform pairs can be caused, for example, by a change in atmospheric or instrumental conditions between acquisition time, or by seasonal changes in the foliage cover. In that case the laser light cannot penetrate to the ground surface, and a mode representing the ground surface will be completely absent.

3.5 *Waveform parameters for forest structure*

Initially, 440 broad-leaved, 62 mixed, and 89 needle-leaved paired waveform pairs were identified from 2363 fitted, February–September waveform pairs. These pairs were filtered according to the following constraints:

- Remove those paired GLAS shots where one or both shots are unimodal.

- Remove those paired GLAS shots where ΔMCH is unfeasibly high, i.e. $> \pm 5$ m.

After applying these data quality filters, 154 broad-leaved, 40 mixed forest, and 44 needle-leaved GLAS pairs remained. The forest parameters derived from these waveform pairs are reported in table 3.

The intensity differences between the canopy waveform returns are given in figure 8. On average, the largest change was detected for broad-leaved forest, followed by a moderate change for mixed forest, while the smallest change occurred for needle-leaved forest, as expected.

Table 3 quantifies changes in forest canopy structure from winter to summer, measured through the use of GLAS. The maximum canopy height for the forest study area was approximately 25 m. The differences in *MCH* from winter to summer were small on average over the three forest types (0.05 m for broad-leaved, −0.06 m for mixed, −0.52 m for needle-leaved). In contrast to *MCH*, the *HOME* parameter was quite sensitive to canopy change. The change in *HOME* was largest (7.22 m) for broad-leaved and decreased for mixed (4.07 m) and needle-leaved (3.15 m) forests.

The ground/canopy ratio (*GRDRT*) also changed most for broad-leaved forest. For the summer waveform, the intensity of the ground return was noticeably less than the canopy return intensity. For the winter waveform, the ground return was much stronger than the canopy return. As a result, the difference of ground/canopy ratio between summer and winter was large (ratio differences of up to 66%). The difference of ground/canopy ratio became smaller for the other forest types (*GRDRT* should be large in winter and small in summer), due to smaller changes in canopy morphology in mixed and needle-leaved forests.

3.6 *Classification of forest types based on waveform-derived forest parameters*

As a first application, but especially as a validation, the changes of the forest parameter values were used to classify general forest waveform pairs into the three forest type classes (broad-leaved, mixed, needle-leaved). For this purpose, the three

Table 3. Forest parameters derived from waveform with $-5\,\text{m} < \Delta MCH < +5\,\text{m}$.

Forest Type	*Season*	*MCH* (m) *(Tree height)*	*HOME* (m) *(Median)*	$GRDRT\left(\frac{Ground}{Canopy}\right)$	ΔI *(Intensity Distance)*
Broad-leaved	Winter	24.65	4.85	1.80	N/A
	Summer	24.70	12.06	0.61	N/A
	Difference	0.05	7.22	−1.20	4.63×10^{-6}
	(%) compared to winter	0.20	148.86	66.67	N/A
Mixed	Winter	26.46	6.13	1.25	N/A
	Summer	26.40	10.20	0.47	N/A
	Difference	−0.06	4.07	−0.78	3.90×10^{-6}
	(%) compared to winter	0.22	66.39	62.40	N/A
Needle-leaved	Winter	24.44	8.54	0.77	N/A
	Summer	23.92	11.70	0.40	N/A
	Difference	−0.52	3.15	−0.36	2.51×10^{-6}
	(%) compared to winter	2.13	36.88	46.75	N/A

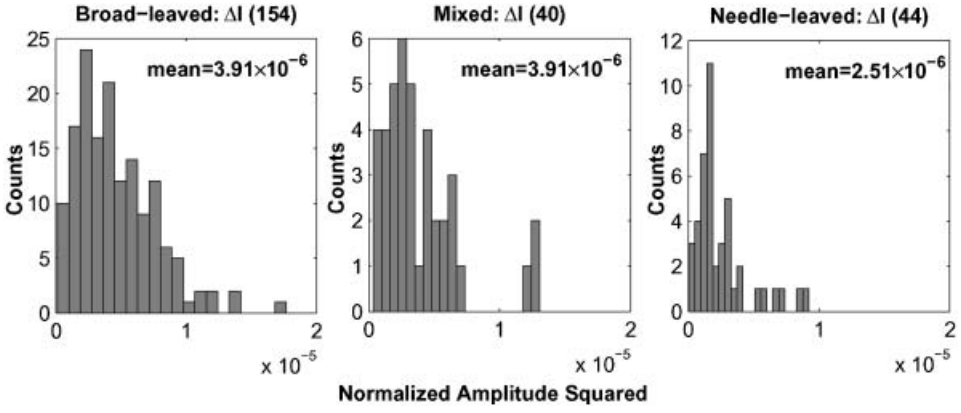

Figure 8. Histograms of canopy intensity differences (ΔI) with $-5\,\mathrm{m} < \Delta MCH < +5\,\mathrm{m}$ in broad-leaved (left), mixed (middle) and needle-leaved (right).

forest classes of the CLC2000 were combined into one forest class. Subsequently, the forest parameters from §3.5 were used to identify the forest species for waveform pairs from this general forest class: broad-leaved, needle-leaved or mixed. The three parameters used were ΔI, $\Delta HOME$ and $\Delta GRDRT$. ΔMCH was not considered to be a classification variable because the differences between February and September were small.

Based on the forest parameters from 442 pairs of summer–winter waveforms, we chose three critical threshold values: *C_I*, *C_HOME* and *C_GRDRT*. These were all defined as the 0.20 quantile of the parameter values found. This procedure gave a value of 2.02×10^{-6} for *C_I*, a value of -0.75 m for *C_HOME* and a value of -1.53 for *C_GRDRT*.

If an intensity difference ΔI was smaller than *C_I*, it was classified as small. The same was applied to $\Delta HOME$ and $\Delta GRDRT$. If the values of $\Delta HOME$ and $\Delta GRDRT$ or the values of $\Delta HOME$ and ΔI were both large, the forest type was classified as broad-leaved. If the values of $\Delta HOME$ and $\Delta GRDRT$ or the values of $\Delta HOME$ and ΔI were both small, the forest type was classified as needle-leaved. In all other cases, the forest type was classified as mixed forest.

The result of this classification was validated (Lillesand *et al.* 2004) by the CLC2000. The accuracy assessment and the classification result are shown in table 4.

Table 4. Confusion matrix and classification results.

	Reference Data (CLC2000)				Classification results			
					Percentage based accuracy		Waveform based accuracy	
Classification Data	*Broad*	*Needle*	*Mixed*	*Total*	Producer	User	Producer	User
Broad	254	17	45	316	80.38	72.78	254/316	254/349
Needle	52	8	11	71	11.27	29.63	8/71	8/27
Mixed	43	2	10	55	18.18	15.15	10/55	10/66
Total	349	27	66	442				
Overall classification accuracy=61.54% and kappa κ=0.57								

The kappa κ value of the classification result was 0.57. This kappa value is not high enough to ensure a reliable differentiation between forest types. Known limitations to this classification method will be explained in §3.7. The use of footprint pairs with larger overlap between single footprints and improved waveform analysis methods, for example the inclusion of slope effects, are expected to improve current classification results. Moreover, additional waveform parameters, introduced by Duong *et al.* (2006) and Ranson *et al.* (2004), can be added to the classification method to potentially improve classification results based on GLAS measurements alone.

3.7 *Recognized problems*

Known limitations of these two GLAS data sets may negatively influence the results. Distances between footprint centres within waveform pairs are between 40 and 90 m (see figure 6). As such, the returned winter and summer waveforms are only directly comparable over homogeneous areas, but many forest waveforms are located in hilly areas where slopes of up to 25° occur (figure 9). The locations of the forest waveforms are displayed along a topographic profile (grey) of the (repeated) ICESat track. Broad-leaved locations (according to CLC2000) are in green, needle-leaved in blue and mixed in red (top panel). The slopes can, by first approximation, be derived from the GLA14 global land surface altimetry product, since both a footprint centre distance and a footprint centre height difference is given for each waveform pair. According to a procedure of Lefsky *et al.* (2005), waveform extent is a function of maximum canopy height and topographic relief. By overlaying the waveform footprint over an SRTM digital elevation model, the range of ground surface elevation within the footprint is determined. This range is the so-called terrain index. The maximum canopy height is then identified by estimating two coefficients based on both the terrain index and the waveform extent. It is clear that slopes directly influence the forest parameters obtained from single waveforms, while local changes in slopes within the area covered by the corresponding waveforms, will make the summer and winter returns less comparable.

Many waveform pairs are removed (see figure 9) from the original 440 waveform pairs, because of unrealistic (changes in) forest parameters: 124 waveform pairs with only one mode and 162 waveform pairs with a reported tree height change exceeding the allowed $-5\,\mathrm{m} < \Delta MCH < +5\,\mathrm{m}$ range. The one-mode waveform pairs either occur in one season (113 pairs with a waveform extent/width and its standard deviation of 11 ± 11 m for the winter, and 23 ± 12 m for the summer) or in both (11 pairs, 8 ± 6 m for the winter and 4 ± 4 m for the summer). Two reasons for the occurrence of one-mode waveforms can be found in errors in the CLC2000 classification, or in changes in the landscape after the CLC2000 classification took place. Large changes in reported tree height may be caused by topographic height differences in the area covered by partially overlapping waveforms.

4. Conclusions and further research

In this paper we have introduced necessary methods for full waveform analysis for deriving forest structures, especially normalization of waveform energy and vertical shifts among waveform pairs, which make waveforms of ICESat repeated tracks comparable. Based on CORINE land cover data, summer–winter waveform pairs were divided into three forest types. It proved possible to derive several parameters

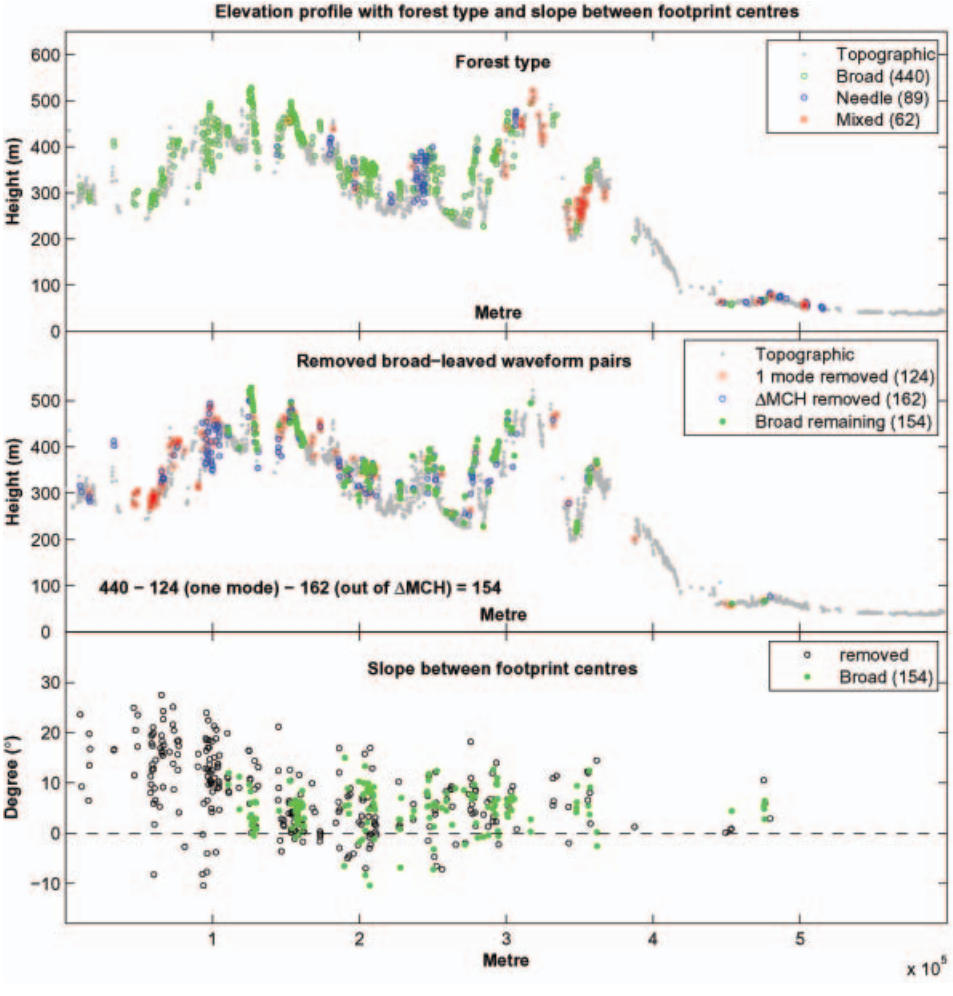

Figure 9. Along track topographic profile (grey) with the three forest types given by the CLC2000 (top). Remaining and removed broad-leaved waveform pairs (second panel). The third panel shows the slopes between the paired footprint centres. Available in colour online.

describing (changes in) forest trees, starting with a Gaussian decomposition of the waveform into single modes. On average, the (change) values obtained for these parameters matched expectation.

We first identified some parameters that can be extracted from waveform data like maximum canopy height, (*MCH*), height of median energy, (*HOME*), ground/canopy return ratio, (*GRDRT*), and canopy intensity difference, (ΔI). As part of the next step we analysed changes in these parameter values. The method showed that we were able to detect and extract the change in forest, or more specifically canopy structure, between different seasons, here winter (leaf-off) and summer (leaf-on). The results indicate that large-footprint, full waveform laser altimetry data may be able to infer changes in, for instance, leaf area index, between different epochs.

Another approach that was employed in this study included the use of tree parameters derived from waveform pairs to classify footprint areas directly into

forest type classes. Preliminary results, with a kappa value of 0.57, provided a baseline against which improvements in the data and methodology can be gauged.

Future works should include a method for correcting slope-induced changes in the waveform results, both for individual waveforms and for waveform pairs. In addition, we expect further improvement by including a neighbourhood analysis, e.g. considering correlation between waveforms and their changes. An individual quality descriptor of the tree parameter values could be obtained from quantifying and propagating errors encountered during the waveform processing. Moreover, tree parameter values should be validated against either data from field measurements or data from other sensors. Finally, the parameter definitions should be refined and validated in order to improve agreement with biophysical characteristics of the forest.

The data set we considered was far from ideal. The ground surface was not flat for most waveform pairs, while the footprint locations from different epochs only partly coincided. In addition, the instruments used for data acquisition differed between the two epochs. Still, we were nevertheless able to find considerable differences between the summer and winter data, with difference values matching the expectations.

Acknowledgements

The authors would like to thank David Korn from the National Snow and Ice Data Center and Gerard Hazeu from Wageningen University for their guidelines and data distribution. We would like to thank our anonymous reviewers for their numerous comments, which considerably helped to increase the quality of this paper. We also would like to thank Merel Keijzer for her correction of the English. This project is funded by the Delft Research Centre Earth.

References

Abshire, J., Zwally, H.J., Shuman, C.A., Hancock, D. and Dimarzio, J.P., 2005, Geoscience Laser Altimeter System (GLAS) on the ICESat mission: On-orbit measurement performance. *Geophysical Research Letters*, **32**, L21S02, doi:10.1029/2005GL024028.

Brenner, A.C., Zwally, H.J., Bentley, C.R., Csatuo, B.M., Harding, D.J., Hofton, M.A., Minster, J.B., Roberts, L.A., Saba, J.L., Thomas, R.H. and Yi, D., 2003, Geoscience Laser Altimeter System Algorithm Theoretical Basis Document: Derivation of Range and Range Distributions from Laser Pulse Waveform Analysis. Available online at: http://www.csr.utexas.edu/glas/atbd.html (accessed 22 February 2006).

Carabajal, C.C., Harding, D.J., Lithcke, S.B., Fong, W., Rowton, S.C. and Frawley, J.J., 1999, Processing of Shuttle Laser Altimeter range and return pulse data in support of SLA02. *International Archives of Photogrammetry and Remote sensing*, **32**(3W14), pp. 67–52.

Corine land cover 2000, 2006, European Environment Agency. Available online at: http://dataservice.eea.eu.int/dataservice/metadetails.asp?id=822 (accessed 5 April 2006).

Dixon, R.K., Brown, S., Houghton, R.A., Solomon, A.M., Trexler, M.C. and Wisniewski, J., 1994, Carbon pools and flux of global forest ecosystems. *Science*, **263**, pp. 185–190.

Drake, J.B., Dubayah, R.O., Clark, D.B., Knox, R.G., Blair, J.B., Hofton, M.A., Chazdon, R.L., Weishampel, J.F. and Prince, S.D., 2002, Estimation of tropical forest structural characteristics using large-footprint Lidar. *Remote Sensing of Environment*, **79**, pp. 305–319.

Dubayah, R., Blair, J.B., Bufton, J.L., Clark, D.B., Jaja, J., Knox, R.G., Luthcke, S.B., Prince, S. and Weishampel, J.F., 1997, The Vegetation Canopy Lidar mission. Land satellite information in the next decade II: Sources and applications. In *Proceedings of the American Society for Photogrammetry and Remote Sensing*, pp. 100–112, Bethesda, MD.

Ducic, V., Hollaus, M., Ullrich, A., Wagner, W. and Melzer, T., 2006, 3D vegetation mapping and classification using full-waveform laser scanning. In *Proceedings of the International Workshop 3D Remote Sensing in Forestry*, 14–15 February 2006, Vienna, Austria.

Duong, H., Pfeifer, N. and Lindenbergh, R., 2006, Full waveform analysis: ICESat laser data for land cover classification. In *Proceedings of the ISPRS Mid-term Symposium, Remote Sensing: From Pixels to Processes*, 8–11 May 2006, Enschede, the Netherlands.

Harding, D.J., Lefsky, M.A., Parker, G.G. and Blair, J.B., 2000, BOREAS Scanning Lidar Imager of Canopies by Echo Recovery (SLICER): Level-3 Data. CD-ROM. Available by special arrangement with Oak Ridge National Laboratory Distributed Active Archive Center, Oak Ridge, Tennessee, USA, http://www.daac.ornl.gov.

Harding, D.J., Lefsky, M.A., Parker, G.G. and Blair, J.B., 2001, Laser altimeter canopy height profiles. Method and validation for closed-canopy, broadleaf forests. *Remote Sensing of Environment*, **76**, pp. 283–297.

Harding, D.J. and Carabajal, C.C., 2005, ICESat waveform measurements of within-footprint topographic relief and vegetation vertical structure. *Geophysical Research Letters*, **32**, L21S10, doi:10.1029/2005GL023471.

Hazeu, G.W., 2003, CLC2000 land cover database of the Netherlands: monitoring land cover changes between 1986 and 2000. *Green World Research*, Wageningen, Alterra, Alterra-rapport 775/CGI-rapport 03-006.

Hofton, M.A., Minster, J.B. and Blair, J.B., 2000, Decomposition of laser altimeter waveforms. *IEEE Transaction on Geoscience and Remote Sensing*, **38**, pp. 1989–1996.

Hofton, M.A. and Blair, J.B., 2002, Laser altimeter return pulse correlation: A method for detecting surface topographic change. *Journal of Geodynamics*, **34**, pp. 477–489.

Jutzi, B., Neulist, J. and Stilla, U., 2005, Sub-pixel edge localisation based on laser waveform analysis. In *Proceedings of the ISPRS WG III/3, III/4, V/3 Workshop 'Laser scanning 2005'*, **39**(3/W19), pp. 109–114.

Lefsky, M.A., Cohen, W.B., Harding, D.J., Parker, G.G., Acker, S.A. and Gower, S.T., 2002, Lidar remote sensing of aboveground biomass in three biomes. *Global Ecology & Biogeography*, **11**, pp. 393–399.

Lefsky, M.A., Harding, D.J., Keller, M., Cohen, W.B., Carabajal, C.C., Espirito-Santo, F.D.B., Hunter, M.O. and Oliveira, R. Jr., 2005, Estimates of forest canopy height and aboveground biomass using ICESat. *Geophysical Research Letters*, **32**, L22S02, doi:10.1029/2005GL023971.

Lefsky, M.A., Harding, D.J., Parker, G.G. and Shugart, H.H., 1999, Surface Lidar remote sensing of basal area and biomass in deciduous forests of eastern Maryland, USA. *Remote Sensing of Environment*, **67**, pp. 83–98.

Lillesand, T.M., Kiefer, R.W. and Chipman, J.W., 2004, Digital image processing. In *Remote Sensing and Image Interpretation* (5th edn) (New York: John Wiley).

Maser, C., 1989, *Forest Primeval – The Natural History of an Ancient Forest* (San Francisco: Sierra Club Books).

National Snow and Ice Data Center, 2005a, Frequently Asked Question. Available online at: http://nsidc.org/data/icesat/faq.html (accessed 22 February 2006).

National Snow and Ice Data Center, 2005b, ICESat mission status. News. Available online at: http://nsidc.org/data/icesat/news.html (accessed 22 February 2006).

Næsset, E., Bollandsås, O.M. and Gobakken, T., 2005, Comparing regression methods in estimation of biophysical properties of forest stands from two different inventories using laser scanner data. *Remote Sensing of Environment*, **94**, pp. 541–553.

PARKER, G.G., 1995, Structure and microclimate of forest canopies. In M. Lowman and N. Nadkarmi (Eds). *Forest Canopies – A Review of Research on Biological Frontier* (San Diego: Academic Press), pp. 73–106.

PERDIGÃO, V. and ANNOVI, A., 1997, Technical and methodological guide for updating CORINE land cover database. Joint Research Centre/European Environment Agency. Available online at: http://www.ec-gis.org/document.cfm?id=197&db=document (accessed on 29 December 2006).

PERSSON, Å., SÖDERMAN, U., TÖPEL, J. and AHLBERG, S., 2005, Visualisation and analysis of full-waveform airborne laser scanner data. In *Proceedings of the ISPRS WG III/3, III/4, V/3 Workshop 'Laser scanning 2005'*, **39**(3/W19), pp. 103–108.

PRESS, W.H., TEUKOLSKY, S.A., VETTERLING, W.T. and FLANNERY, B.P., 1992, *Numerical Recipes in C: The Art of Scientific Computing* (New York: Cambridge University Press).

RANSON, K., SUN, G., KOVACS, K. and KHARUK, V., 2004, Land cover attributes from ICESat GLAS data in central Siberia. *International Geoscience and Remote Sensing Symposium, Anchorage, AK, 20–24 September 2004, IGARSS 2004: IEEE International Geoscience and Remote Sensing Symposium Meetings 1–7*, **34**, pp. 753–756.

REITBERGER, J., KRZYSTEK, P. and HEURICH, M., 2006, Full-waveform analysis of small footprint airborne laser scanning data in the Bavarian forest national park for tree species classification. In *Proceedings of the International Workshop 3D Remote Sensing in Forestry*, 14–15 February 2006, Vienna, Austria.

WAGNER, W., ULLRICH, A., DUCIC, V., MELZER, T. and STUDNICKA, N., 2006, Gaussian decomposition and calibration of a novel small-footprint full-waveform digitising airborne laser scanner. *ISPRS Journal of Photogrammetry & Remote Sensing*, **60**, pp. 100–112.

ZWALLY, J., *et al.*, 2002, ICESat's laser measurements of polar ice, atmosphere, ocean, and land. *Journal of Geodynamics*, **34**, pp. 405–445.